Evolution of Ocean Temperature and Ice Volume Through the Mid-Pleistocene Climate Transition

H. Elderfield,* P. Ferretti,† M. Greaves, S. Crowhurst, I. N. McCave, D. Hodell, A. M. Piotrowski

Earth's climate underwent a fundamental change between 1250 and 700 thousand years ago, the mid-Pleistocene transition (MPT), when the dominant periodicity of climate cycles changed from 41 thousand to 100 thousand years in the absence of substantial change in orbital forcing. Over this time, an increase occurred in the amplitude of change of deep-ocean foraminiferal oxygen isotopic ratios, traditionally interpreted as defining the main rhythm of ice ages although containing large effects of changes in deep-ocean temperature. We have separated the effects of decreasing temperature and increasing global ice volume on oxygen isotope ratios. Our results suggest that the MPT was initiated by an abrupt increase in Antarctic ice volume 900 thousand years ago. We see no evidence of a pattern of gradual cooling, but near-freezing temperatures occur at every glacial maximum.

The deep-ocean sediment oxygen isotopic composition record ($\delta^{18}O_C$), commonly considered to be a record of global ice volume and thus a chronicle of ice ages, also is "heavily contaminated" (*1*, *2*) by the effect of deep-water temperature variability. The contributions of ice volume and temperature to $\delta^{18}O_C$ have been debated for more than 40 years [e.g., (*1–5*)], and definition of the trajectories that each followed during the mid-Pleistocene transition (MPT) has been elusive. Here, we present a high-resolution record of deep-water temperature, which we constructed based on foraminiferal Mg/Ca paleothermometry (see supplementary text and fig. S1). Only one previous deep-sea temperature record extending over the MPT and obtained independently of oxygen isotopes exists, and this is at orbital-scale resolution from the North Atlantic using Mg/Ca ratios from benthic foraminifera (*6*). However, it has been recognized recently that Mg/Ca ratios of epifaunal benthic foraminifera are affected by carbonate saturation effects (*7*, *8*), requiring a "regional calibration," and, consequently, the reliability of this approach has been both challenged (*9*) and defended (*10*). The increasing interest in applying inverse models to deconvolve temperature and ice volume in climate records [e.g., (*11–14*)] adds to the interest in separating these signals from the oceanic sediment record using geochemical methods.

Previously, we carried out a calibration study using the shallow-infaunal benthic foraminifera *Uvigerina* spp., showing that it is little affected by bottom-water carbonate saturation, and generated a low-resolution benthic temperature record for the past 440 thousand years (ky) (*15*). We now have generated a 1.5-million-year record of deep-sea temperature and sea level with a resolution (≤1000 ky) sufficient to define their behavior over the period of the MPT, including a comparison with the climate of the last 800 ky derived from ice-core records (*16*) and information on changes in ocean carbon chemistry.

The site studied—Ocean Drilling Program (ODP) leg 181, site 1123—is located on the Chatham Rise, east of New Zealand at 41°47.15′S, 171°29.94′W, at a depth of 3290 m (fig. S2). It lies under the Deep Western Boundary Current (DWBC) that feeds the Pacific and comprises Lower Circumpolar Deep Water (CDW), which forms from dense waters sinking around Antarctica, particularly cold waters from the Weddell and Ross seas and Adelie Coast. The modern hydrography of the site shows a slight contribution from North Atlantic Deep Water (NADW) expressed by a small salinity anomaly marker (*17*). More than half of the flux of cold bottom water entering the major basins of the world ocean does so through the Southwest Pacific Ocean, as the Pacific DWBC (*17*, *18*). CDW is drawn to the surface by upwelling with descending return flows south of the upwelling as Antarctic Bottom Water (AABW) and north of it as Antarctic Intermediate Water. The connection of this site to the regions where deep Antarctic water masses form enables comparison with Southern Ocean and Antarctic atmospheric records and is important for determining the role of the deep ocean in climate evolution.

Benthic $\delta^{18}O_C$, deep-sea temperature, and Antarctic temperature. We determined $\delta^{18}O_C$ and Mg/Ca on 1650 and 1485 samples of *Uvigerina* spp. (supplementary text, table S1, and Fig. 1). Data are also archived at doi:10.1594/PANGAEA.786205 The $\delta^{18}O$ data were correlated to an orbitally tuned benthic $\delta^{18}O$ stack, LR04 (*19*), to provide an initial time scale. The $\delta^{18}O$ record of benthic foraminiferal calcite extends from marine isotope stage (MIS) 50, 1550 thousand years ago (ka), to the Holocene (Fig. 1A). It shows features in common with the LR04 stack with stable interglacial values (except for the anomalous interglacials MIS 5, 9, and 11) and lower glacial values before MIS 22.

There are, however, differences between our $\delta^{18}O$ record and the LR04 stack, in particular over the period thought to encompass the MPT. Benthic $\delta^{18}O_C$ shows an abrupt increase from about 950 ka to 870 ka, whereas LR04 shows a more gradual increase to values 0.5 per mil (‰) lighter than for ODP 1123. This is not an artifact of benthic species analyzed, because we have verified this observation by measuring $\delta^{18}O$ also on the epibenthic species *Cibicidoides wuellerstorfi* (fig. S3A).

What is the importance of this difference? LR04 is thought to represent a global average from which regional variability has been removed. Nevertheless, LR04 is not an area-weighted stack and is biased to the Atlantic Ocean and eastern equatorial Pacific. Only one site samples the major flow to over half the volume of the world ocean and that is ODP 1123. The LR04 stack is widely used, but to discuss the implications for changing global ice volume we need to delve further. Because of the possible bias in the stack, it makes more sense to compare our site 1123 record with a few other high-quality records from the world oceans. The more abrupt change in $\delta^{18}O_C$ is seen in some records but not others (fig. S3, B to D). Some records show a stepped increase in $\delta^{18}O_C$ over the period 1000 to 600 ka. If interpreted as ice volume, $\delta^{18}O_C$ shows that the first large ice sheet was at MIS 16 in the Atlantic but at MIS 22 in the Pacific, as indicated by ODP 1123. It is likely that the difference of individual sites from each other and from LR04 reflects changes in hydrography, smoothed in the stack.

The benthic $\delta^{18}O_C$ record has a temperature component and a seawater $\delta^{18}O$ component, and the latter may reflect a combination of a global ice volume signal and a local hydrographic signal relating, for example, to changes in proportions of colder low $\delta^{18}O$ AABW versus warmer high $\delta^{18}O$ NADW. If our signal may reflect "local" hydrographic changes, those changes are related to Antarctica because deep-water masses at site 1123 originate from waters sinking around Antarctica. Detailed records in addition to those in Fig. 1 at key hydrographic locations would be required to fully assess variability in the global seawater $\delta^{18}O$ signal. Our assessment is that the hydrographic component at the site of 1123 is small: (i) benthic isotopic depth profiles at the site of ODP 123 are related to the structure of water masses at present and inferred for the past, with no apparent changes in the depths of water-mass boundaries between glacial and interglacial states (*17*); (ii) estimates of oxygen isotopic composition of seawater ($\delta^{18}O_W$) from corals and

Godwin Laboratory for Palaeoclimate Research, Department of Earth Sciences, University of Cambridge, Downing Street, Cambridge CB2 3EQ, UK.

*To whom correspondence should be addressed. E-mail: he101@cam.ac.uk

†Present address: Consiglio Nazionale delle Ricerche, Istituto per la Dinamica dei Processi Ambientali (CNR-IDPA), Calle Larga Santa Marta 2137, Venice I-30123, Italy.

pore water modeling discussed below show global values. Ideally, what is needed is a global array of seawater $\delta^{18}O$ records that could be stacked to produce a mean ocean $\delta^{18}O$ signal.

There is also considerable millennial and sub-millennial scale variability in the records, more in Mg/Ca than $\delta^{18}O_C$ (supplementary materials and Fig. 1, A and B). To aid in comparison, oxygen isotope and Mg/Ca data have been smoothed in the time domain using a Gaussian filter having a total width of 5 ky. The range in Mg/Ca of *Uvigerina* spp. is narrow (~0.8 to 1.3 mmol/mol) but shows clearly a different overall pattern than $\delta^{18}O$ (Fig. 1B).

Mg/Ca was converted to temperature using the sensitivity previously determined (*15*) of 0.1 mmol/mol per °C. This is based on 56 core top samples that show a statistically significant correlation between Mg/Ca and bottom-water temperature (fig. S4). Results show a temperature range from about 3°C in the warmest interglacial to a reasonably constant value of about –1.5 to –2°C for the glacials (Fig. 1B), which we discuss later, with an estimated error of about ± 1°C (supporting materials).

There is a striking similarity between our deep-water temperature record and the 800-ky record of atmospheric temperature above Antarctica from ice cores (*16*) (Fig. 1B). For this comparison, we converted Mg/Ca temperature data to units of standard deviation and transposed them to the EDC3 (Epica Dome C ice core) time scale (*20*). The pattern seen in the ice-core δD (deuterium isotope-based temperature) record is matched by the Mg/Ca–based deep-sea temperature: (i) glacial temperatures are similar throughout this deep-sea record, (ii) interglacial temperatures are cooler prior to 450 ka, and (iii) interglacials 5.5, 7.5, 9.3, and 11.3 are exceptionally warmer.

The distinction between interglacial bottom-water temperature before and after ~450 ka seen in our record and in the ice-core atmospheric record is also similar to a sub-Antarctic Atlantic sector record of sea surface temperature using an alkenone proxy (*21*) and of the oxygen isotopes of that site (*22*). It is also recognized in model-based deconvolution of global deep-sea temperature from the benthic $\delta^{18}O$ stack (*11*). However, it is not seen in the North Atlantic benthic Mg/Ca record referred to earlier (*6*). It is unclear whether this reflects the linkage of that site to hydrographic conditions associated with changing proportions of NADW and AABW or is somehow a mixed signal related to a contribution from carbonate ion as discussed earlier (*9*, *10*).

Glacial-interglacial model comparisons (*23*) suggest that Antarctic temperature changes represent global-scale temperature changes with a polar amplification factor of ~2: glacial-interglacial temperature change (Antarctic/Global) = 2.07. The comparison of Antarctic and our deep-sea temperature data shows the same amplification (Antarctic/deep sea) = 2.1 ± 0.08 (fig. S5). Therefore, it seems that the temperature of the bottom water reflects the air temperature at southern high latitudes and thus Southern Ocean surface temperatures, aided by upwelling and surface mixing of CDW.

Ice volume and sea level. Given Mg/Ca, rearrangement of the paleotemperature equation allows changes in the $\delta^{18}O_W$ ($\Delta\delta^{18}O_W$) to be calculated [(*15*) and supplementary text). We made two tests of the methodology. First, we compared our results over the past 250 ky with estimates of global sea level made from accurately dated corals. The coral method is independent of orbital-based $\delta^{18}O_C$, whereas other sea-level methods rely on comparison with benthic $\delta^{18}O$. Considering that propagation of estimated temperature and $\delta^{18}O_C$ uncertainties results in an error in $\delta^{18}O_W$ of ±0.2 ‰, our results (fig. S6) show excellent agreement with compilations of coral data (*24*, *25*). Second, it can be seen that

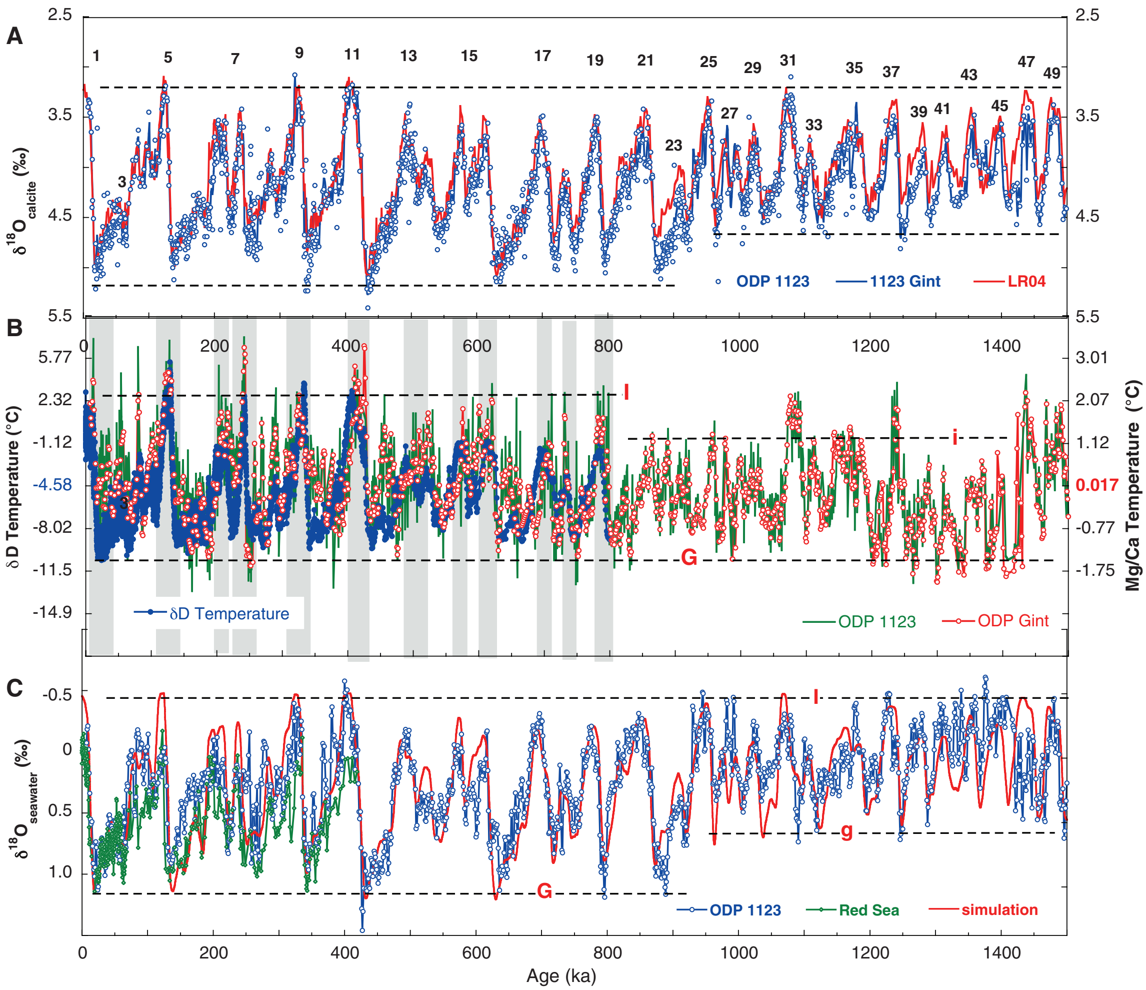

Fig. 1. Records on the LR04 chronology of (**A**) The LR04 benthic $\delta^{18}O$ stack (*19*) (red); ODP 1123 benthic $\delta^{18}O$ (original data in blue open symbol and smoothed record with a Gaussian filter having a span of 5 ky as a line in blue); (**B**) Record on the EDC3 chronology (*20*) of ODP 1123 benthic Mg/Ca temperature (original data in green and smoothed record with a 5-ky Gaussian filter red) and Antarctic temperature (*16*) (blue). Data were converted to units of standard deviation. Ordinate axes show mean temperatures (in red and blue) and also values of mean ±3σ°C. MIS is labeled for orientation in Fig. 1A and in shaded panels in Fig. 1B. (**C**) Ice volume ($\delta^{18}O$ of seawater) derived from ODP 1123 Mg/Ca and $\delta^{18}O_C$ (blue) compared with the simulation of Bintanja *et al.* (*11*) (red) and record from the Red Sea (*28*) (green).

the change in $\delta^{18}O_W$ since the Last Glacial Maximum is ~1.2‰ for 120 m of sea-level change, identical to the value of 1.1 ± 0.1‰ derived from porewater modeling at this Chatham Rise site and similar to global estimates (*26*). This exercise goes some way toward addressing the issue discussed earlier on the influence of local hydrography on the site 1123 $\delta^{18}O_C$ record.

One further factor in estimating sea level by this approach is the simplifying assumption of a constant $\delta^{18}O_W$ through a glacial cycle, whereas $\delta^{18}O$ of ice ($\delta^{18}O_I$), and $\delta^{18}O_W$, will increase as the ocean is progressively depleted of ^{16}O (*27*). Assumption of $\delta^{18}O_W$ based on a constant $\delta^{18}O$ of ice has little impact on derivation of sea level estimated from $\delta^{18}O_W$ records during the start of a glacial cycle but has a larger impact at full glaciation (fig. S7). Here, we have used $\delta^{18}O_I$ = –40‰. On this basis, we have calculated the $\delta^{18}O_W$ and, assuming that this reflects global ice volume, derived a sea-level reconstruction since 1550 ka and compared it with a recent simulation and record of sea-level change (*11*, *28*) (Fig. 1C).

First, we estimate the contributions of $\delta^{18}O_W$ and temperature to $\delta^{18}O_C$, a subject of long-standing debate (*1*–*4*). Temperature has been scaled as $\delta^{18}O_T$, and all data are plotted as "cold upwards" to show the evolution of temperature and ice volume from interglacial to glacial conditions (Fig. 2, A and B). We see different behavior between 100,000-year (Fig. 2, A and B) and 41,000-year (Fig. 2, C and D) cycles, periodicities consistent with the tempo of variations in orbital eccentricity and obliquity. This exercise shows that the increase in $\delta^{18}O_W$ (ice volume) during eccentricity cycles proceeds slowly throughout some glacial periods to a maximum value that corresponds to a ~70% contribution to $\delta^{18}O_C$, but there are also periods of rapid change. In contrast, $\delta^{18}O_T$ cools early in each glacial cycle by about 0.8‰. The contrast between the rapid temperature decrease completed one-third of the way through each $\delta^{18}O_C$ cycle and the more gradual lagged increase in ice volume has two implications. One is that, as suggested by the simulation of Bintanja *et al.* (*11*), rapid deep-ocean cooling preceded slower buildup of ice sheets. The other is that the near constancy of glacial $\delta^{18}O_T$ (red dashed line in Fig. 2, A and B), irrespective of the strength of individual $\delta^{18}O_C$ maxima, suggests that glacial cooling is limited by water's freezing temperature such that glacial temperatures have remained nearly constant since at least 1500 ka. This analysis also shows that the saw-tooth character of the oxygen isotope cycles is a feature of the $\delta^{18}O_W$ component of the record—slow ice-sheet buildup and rapid decay—whereas the temperature component resembles a square wave function resulting from the limitation of the temperature fall during the early stages of ice-sheet growth.

The records over obliquity cycles before about 1 million years ago show a much weaker role for ice volume because of smaller ice sheets. The $\Delta\delta^{18}O_W$ component of the record is 0.77 ± 0.16 ‰ for MIS 24 to 50, compared with 1.09 ± 0.17‰ over MIS 2 to 22 (fig. S8), equivalent to a sea-level fall from ~60 to 90 m for the obliquity cycles to ~90 to 125 m for the eccentricity cycles. However, $\Delta\delta^{18}O_T$ shows no such contrast and averages 0.80 ± 0.14‰ over all glacials sampled, equivalent to cooling of about 3°C to –2°C (Fig. 2C).

This study emphasizes the point that benthic $\delta^{18}O$ is not a direct proxy of ice volume or sea level (*1*–*3*). Because the LR04 stack (*19*) is often taken as a proxy for ice volume, it is interesting that the temperature component of this record may approach as much as 50% of the range in $\delta^{18}O_C$.

Timing of MPT events. With this assessment of the relative contributions of temperature and ice volume to $\delta^{18}O_C$, it is possible to address what was the sequence of events leading to the MPT. A review of $\delta^{18}O_C$ records (*5*) has shown that the MPT began 1250 ka and was complete by 700 ka, with low-frequency (i.e., 100 ky) power emerging at about 1250 ka followed by a lull centered on 1000 ka, with reemergence of power beginning at ~900 ka. Wavelet analysis of our $\delta^{18}O_C$, $\delta^{18}O_W$, and Mg/Ca records using Sowas software (*29*, *30*) shows somewhat similar but more complex patterns (Fig. 3). In the $\delta^{18}O_W$ record, the highest spectral power in the 100-ky band develops from 650 ka. Temperature gains power in this band over 400 to 100 ka, whereas $\delta^{18}O_C$ is a "fusion" of the two with lower yet significant power from 900 ka and intensified power from ~650 ka.

The record of glacial deep-ocean temperatures over this period is similar to that which characterizes glacials at this site throughout the Pleistocene. As shown above, rapid deep-ocean cooling within each glacial-interglacial cycle preceded slower buildup of ice sheets, but there is no evidence of progressive cooling throughout the record; glacial to interglacial temperature change ($\Delta\delta T$)

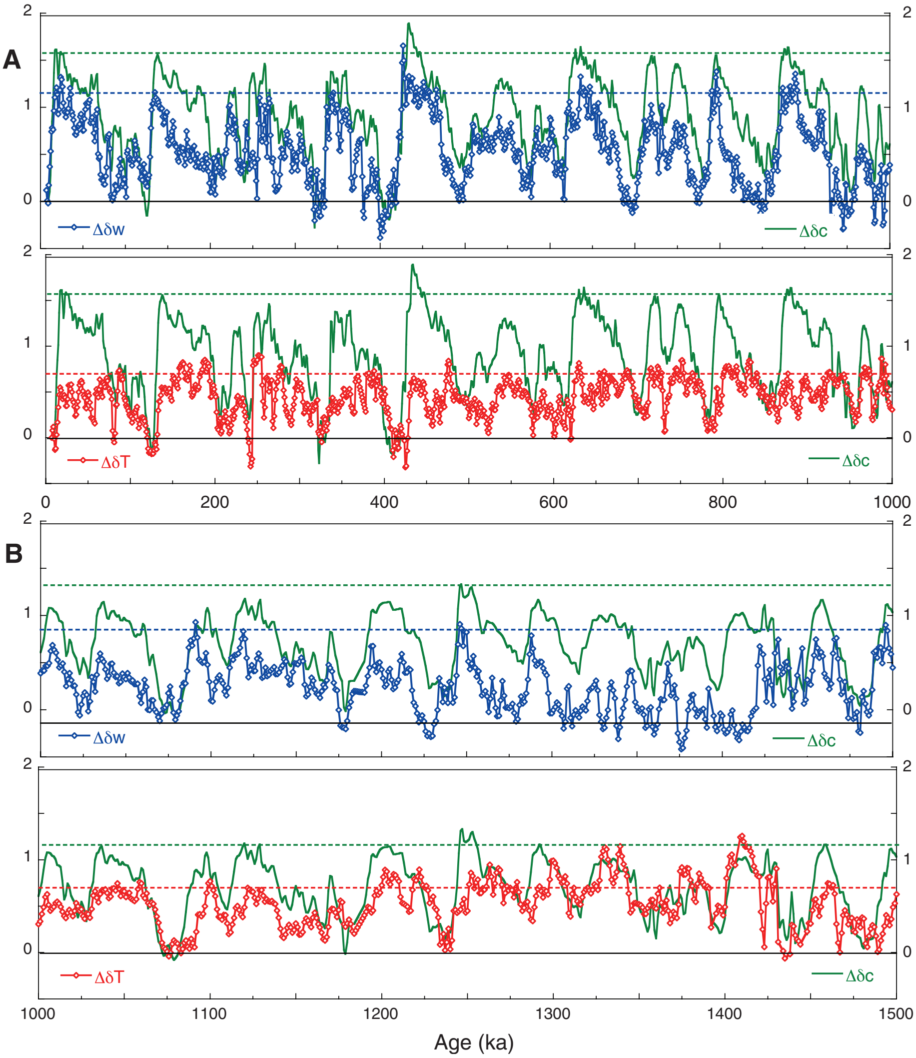

Fig. 2. Comparison of contributions of changes in ice volume, ΔδW (blue) and temperature, ΔT (red) to benthic $\delta^{18}O$, ΔδC (green): (**A**) for 0 to 1000 ka and (**B**) for 1000 to 1500 ka. Data are plotted as "cold upwards." Temperature converted to δT ‰ units using 0.25 ‰ per °C/0.1 mmol/mol per °C. Histogram of data shown in fig. S8.

is constant at about 0.8‰ over every glacial cycle except for the warm interglacials. Temperature decline cannot therefore be the unique cause of increased ice volume across the MPT. However, a characteristic of the eccentricity cycles, less so for obliquity, is the persistence of near-freezing temperatures over most of the periods of ice growth; the longer slow growth of ice sheets occurred when cold temperatures persisted for longer.

In contrast to temperature, the change in ice volume is late within the MPT period, and its timing coincides with the so-called 900-ka event at the onset of MIS 22 (Figs. 1C and 4A). Before this event, the record oscillates between mild glacials (g) and lukewarm interglacials (i), suggesting that the climate system varied between two quasistable climate states (*31*, *32*). After MIS 25, ice volume increased sufficiently to weaken interglacial MIS 23 and initiated the onset of full glacial conditions (G) beginning with MIS 22 (~900 ka). MIS 22 marks an abrupt increase in glacial $\delta^{18}O_W$ values, indicating a transition to maximum ice volume that has characterized most full glacial (G) stages since ~900 ka. Our results suggest that the MPT represents an abrupt reorganization of the climate system as opposed to a long-term trend toward increased ice volume and colder temperatures as previously thought (*5*). The duration of the glacial cycle lengthens with MIS 22 to 24, but the strong increase in the 100-ky power is delayed until ~650 ka (MIS 16), which is where power in $\delta^{18}O_W$ reaches its maximum (Fig. 3). From 900 to 400 ka, the climate system varied between three end-member climate states: lukewarm interglacials (i), mild glacials (g), and full glacials (G) [after Paillard (*31*)]. It is not until 400 ka during the mid-Brunhes event that full interglacial conditions (I) emerged, most vividly expressed in the deep-sea temperature record.

Although suggestions that the MPT was a gradual transition are shown in a number of benthic $\delta^{18}O$ records, our evidence for a more abrupt transition comes from seawater $\delta^{18}O_W$ (Fig. 1C). We attribute this difference to hydrographic contributions to $\delta^{18}O_C$.

What conditions may have led to the abrupt increase in continental ice volume during MIS 22? Examination of the sea-level (ice volume) record across the MPT (Fig. 4A) shows that the critical step in ice-volume variation was associated with the suppression of melting in MIS 23, followed by renewed ice growth in MIS 22 to yield a very large ice sheet with 120 m of sea-level lowering (Fig. 4A). This period is associated with an anomalously low Southern Hemisphere summer insolation across the minor melting MIS 23. We suggest that this configuration suppressed melting and allowed larger ice-sheet growth that led to the first prolonged 100-ky glacial cycle comprising MIS 22 to 24. Because the low summer insolation occurred in the Southern Hemisphere, we suggest that the cause of ice volume increase at 900 ka lay in Antarctica.

Cross-spectral analysis of our records shows that at eccentricity periods, $\delta^{18}O_C$ lags Mg/Ca (temperature) by ~12 ky, as found earlier (*15*, *33*), and $\delta^{18}O_W$ lags Mg/Ca by ~21 ky with, as expected, $\delta^{18}O_C$ intermediate between $\delta^{18}O_W$ and temperature; see supplementary text and fig. S9 for discussion of the phase relationship between orbital eccentricity and Mg/Ca (temperature).The 41-ky bandpass filtered data show, as in (*33*), in-phase relationships between all measured parameters, whereas the 100-ky bandpass filtered data shows considerable variability in phase (fig. S9). Over the period from ~1100 to 750 ka, where 100-ky power is weak, the lag increases to the extent that $\delta^{18}O_C$ and $\delta^{18}O_W$ are out of phase with δT at 900 ka, after which there is a transition to strong 100-ky cycles from ~700 ka. Thus, the "lock in" to a late Pleistocene 100-ky phase relationship occurs at around 750 ka, with some variation before then.

The notion that the Antarctic ice sheet was inactive throughout the Pleistocene is not supported by our work or by records emanating from the margins of Antarctica and some models (*34*–*37*). Raymo *et al*. have proposed a more active East Antarctic ice sheet before 1 Ma with its expansion and development of the present less-active regime at the MPT (*34*). Their proposal—that at the MPT, "marine-based ice-sheet margins replaced terrestrial ice margins around East Antarctica, resulting in a shift to in-phase behavior of northern and southern ice sheets" (*34*)—is borne out by drill cores on the edge of the Ross Sea (*35*, *37*). Pollard and De Conto (*36*) model an increase in West Antarctic Ice Sheet ice volume of ~10^7 km^3 (~17 m of sea level) across the MIS 25 to 22 transition.

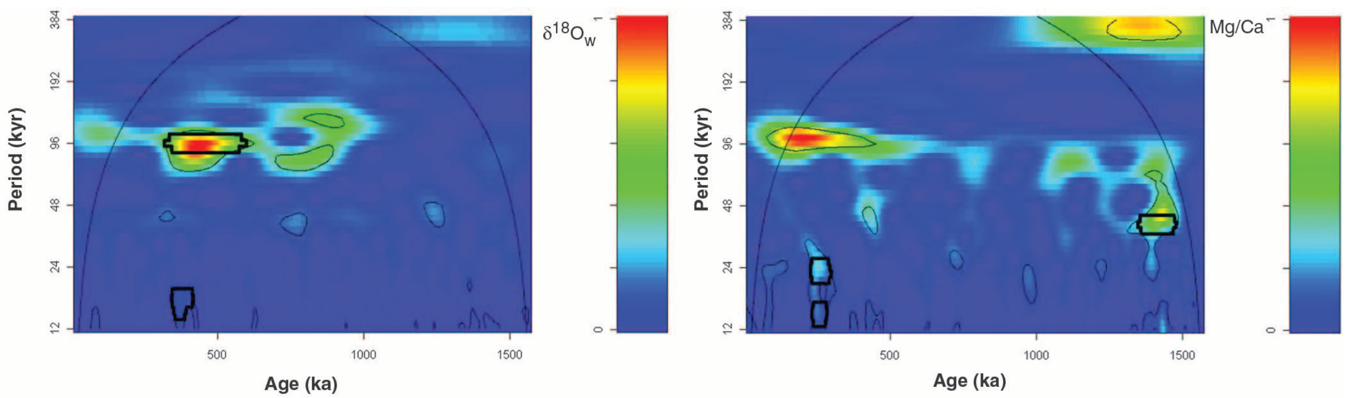

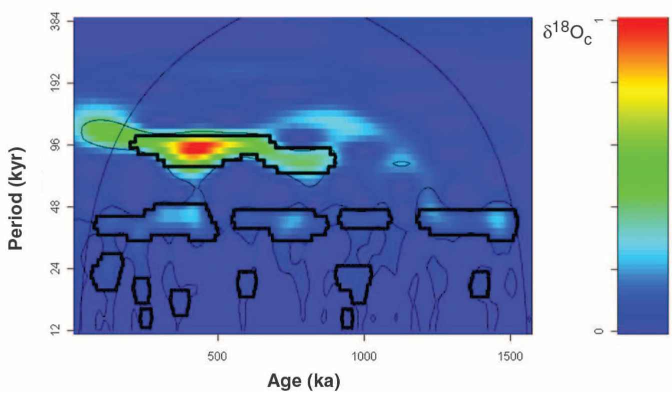

Fig. 3. Wavelet plots using Sowas software (*29*, *30*). These plots make it clear that the 100-ky cyclicity is most powerful in $\delta^{18}O_W$ over 700 to 300 ka, and in the temperature 400 to 100 ka, with the calcite $\delta^{18}O$ a "fusion" of the two.

Carbon chemistry and ocean circulation. The rapid increase in ice volume at MIS 22 is associated with a large perturbation to ocean carbon chemistry (*38–40*), as reflected in the most depleted benthic $\delta^{13}C$ values in the Pacific and Atlantic over the past 5 million years (*36–38*) This is also seen in the ODP 1123 record (Fig. 4A and Fig. 5). Because it is represented in many records, some authors have argued that this decrease in oceanic $\delta^{13}C$ is a global event. It has also been argued that benthic $\delta^{13}C$ values begin to decline much earlier than at MIS 22, at about 1.5 Ma (*41–43*), reaching a minimum at 900 ka and increasing to about 500 ka. However, our results suggest that the carbon isotope excursion was associated with an abrupt reorganization of the climate system rather than a long-term trend, characterized by the most depleted $\delta^{13}C$ values at the MPT within a record of otherwise rather similar glacial values (Fig. 5). Therefore we will focus first on the extreme depletion in $\delta^{13}C$ at the MPT and next consider its glacial-interglacial cycles.

We can dismiss the hypothesis that the $\delta^{13}C$ record for this site, which is based on an infaunal foraminiferal species, is depleted relative to bottom water and reflects productivity-related changes in pore-water composition. This is because paired *Cibicidoides-Uvigerina* data (fig. S10) show a constant offset of ~0.9‰ between the epifaunal and infaunal species. The *Uvigerina* spp. $\delta^{13}C$ record cannot therefore reflect changes in metabolic CO_2 at the depth of this ODP site. Given this, we can explore interpretations of the benthic $\delta^{13}C$ record, first exploiting the ice-volume record that we have derived.

Before 900 ka, sea-level lowstand during glaciations was ~70 m below the present. MIS 22 represents the first time in millions of years that sea level dropped to 120 m, exposing shelf break and upper-slope deposits (*38*). Marine organic carbon (with $\delta^{13}C$ of ~–18‰) exposed on shelves and transferred to seawater would lower benthic $\delta^{13}C$. The depletion in $\delta^{13}C$ compared with "normal" glacials (for example, MIS 20, 24, and 26) is about 0.2‰, equivalent to about 300 Pg of carbon. A test of this hypothesis is to examine the relationship between $\delta^{13}C$ and $\delta^{18}O_W$. Ice volume and $\delta^{13}C$ look very tightly coupled in Fig. 4A and Fig. 5. This strong link between $\delta^{18}O_W$ and $\delta^{13}C$ suggests that sea level and/or circulation is involved in glacial-interglacial $\delta^{13}C$ changes. This is a more likely cause than change in the terrestrial carbon reservoir resulting from global aridity, as originally conceived by Shackleton (*44*). The 41-ky bandpass filtered data show (as above for other climate variables) that $\delta^{18}O_W$ and $\delta^{13}C$ are closely in phase (fig. S9) but the responses in the 100-ky band after 900 ka show a small lead of $\delta^{13}C$ to $\delta^{18}O_W$. Taken at face value, this does not support the shelf hypothesis over 100-ky time scales.

The second interpretation, argued indirectly from several avenues [summarized in (*45*)], is that benthic $\delta^{13}C$ is controlled by the hydrographic properties of site ODP 1123 (mostly in addition to fluctuations in the marine C reservoir) affected by changes in global thermohaline circulation with or without concomitant change in nutrients (*44*, *45*). As discussed above, differences between $\delta^{18}O_C$ records of site 1123 and the LR04 stack provide some evidence of a secondary hydrographic control. We have tested this hypothesis using Nd isotopes that act as a hydrographic tracer largely unaffected by changes to organic carbon systematics. Northern source waters have a more negative εNd than southern source waters (*46*). If the $\delta^{13}C$ changes reflect changes in proportions of water masses, we would anticipate that they should be associated with concomitant changes in εNd. We examined three periods: over the last deglaciation, the warm interglacial 100-ky cycles MIS 12 to 10, and

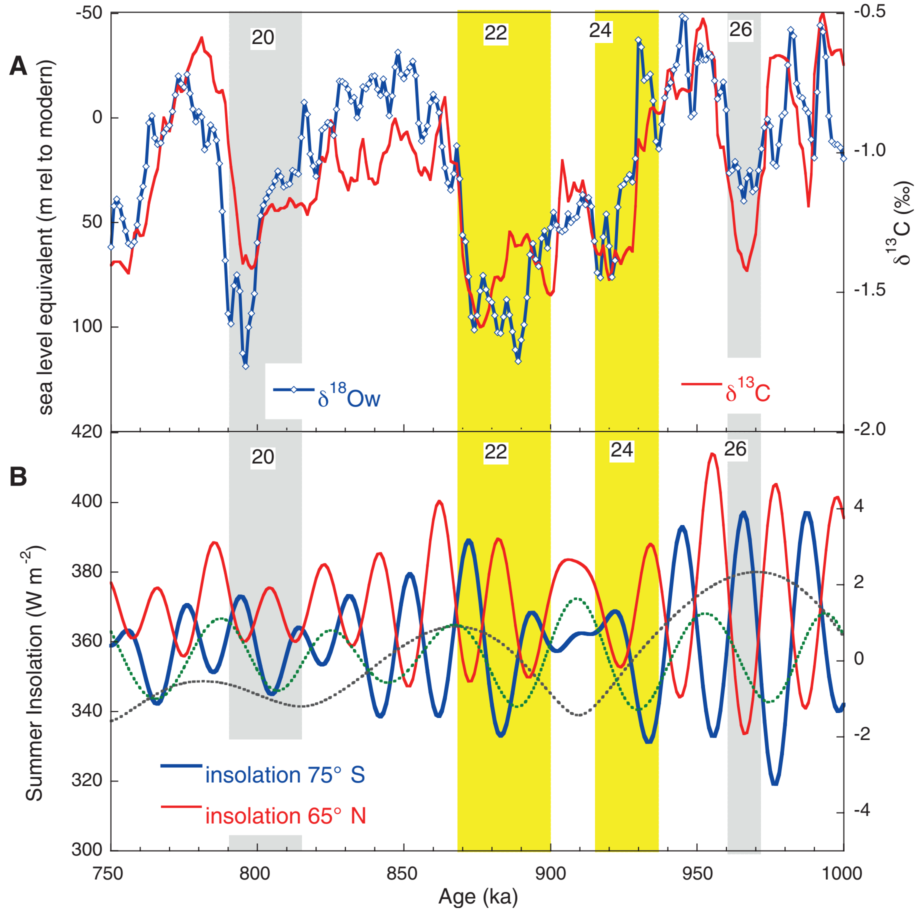

Fig. 4. (**A**) Record over 750 to 1000 ka showing age of the MPT at MIS 22 inferred from $\delta^{18}O_W$ (sea level) (blue). Also shown is benthic $\delta^{13}C$ (red). MIS with boundaries taken from LR04 (*19*) are labeled and shown in shaded panels for orientation. (**B**) Normalized orbital variation in energy received by Earth at eccentricity and obliquity (blue and green dashed lines) and Northern and Southern Hemisphere (red and blue lines) insolation frequencies for the period 1 Ma to 800 ka; note the antiphase relation between obliquity and a wide Southern Hemisphere insolation peak at 920 to 900 ka.

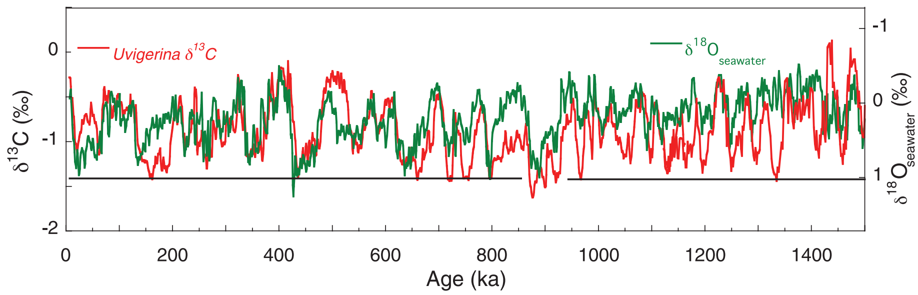

Fig. 5. Record of benthic $\delta^{13}C$ and $\delta^{18}O$ of seawater. $\delta^{13}C$ at MIS 22 is most depleted of benthic $\delta^{13}C$ values in the Pacific and Atlantic over the past 5 million years (*42*).

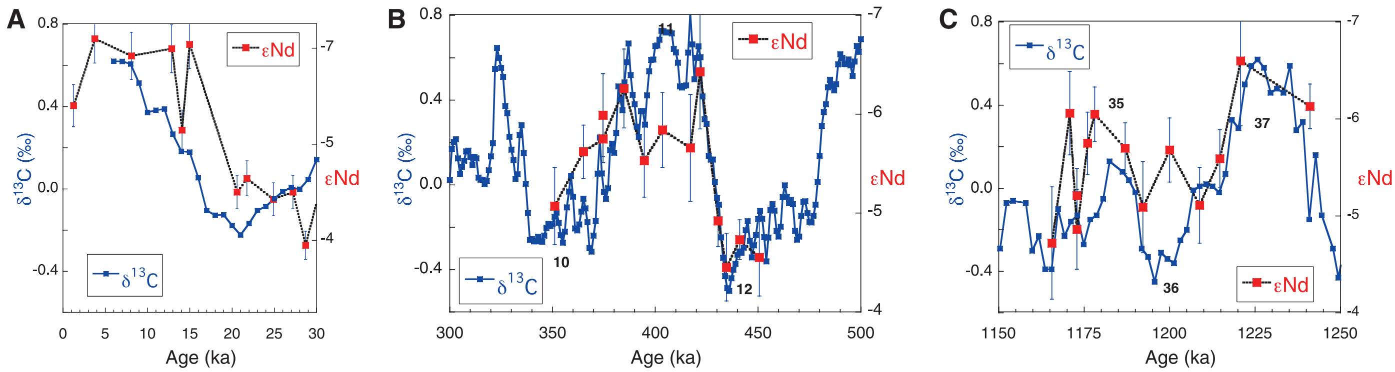

Fig. 6. Records of εNd (red) and $\delta^{13}C$ (blue) for three periods within core ODP 1123: (**A**) 0 to 30 ka, (**B**) 300 to 500 ka, (**C**) 1150 to 1250 ka. All show that in warm periods, εNd is more negative, suggesting greater NADW influence.

the obliquity cycles MIS 38 to 35 (Fig. 6). In each case, the records of εNd and $\delta^{13}C$ are similar in form, with a small range in εNd from about –7 at interglacial stages to –4 at glacial stages. This implies that the 100-ky and 40-ky cycles of $\delta^{13}C$ are associated with changes in deep-ocean circulation, perhaps a decrease in glacial export of NADW relative to CDW coupled with changes in Southern Ocean deep-water ventilation (*17*, *33*, *39*). However, given the location of ODP 1123, there is little scope for large variations in end members.

Plots of the relationship between εNd and $\delta^{13}C$ data reveal that large changes in the oceanic carbon reservoir occur in addition to those in $\delta^{13}C$ that are associated with changes in εNd (fig. S11). Of the glacial-interglacial offset in $\delta^{13}C$ of about 1‰ (Fig. 5), about half is associated with circulation and half with carbon reservoir. A whole-ocean decrease in $\delta^{13}C$ of 0.4‰ would represent about half of the $\delta^{13}C$ change over glacial-interglacial cycles and would require transfer of about 500 Pg of terrestrial carbon to the oceans, together with an increase in atmospheric CO_2 of 45 parts per million by volume before compensation.

Importance. Most hypotheses account for the origin of the MPT as a response to long-term ocean cooling, perhaps because of lowering CO_2 (*5*). Data of CO_2, directly from ice cores and indirectly from the $\delta^{11}B$ proxy (*47*) (fig. S12), are as yet too sparse to determine the respective roles of temperature and of the carbon system. We have defined the timing of initiation of the MPT as an abrupt event centered on MIS 24 to 22 (the 900-ka event). The descent into longer glacials, the MPT, appears to have begun in MIS 23 by suppression of substantial melting of the ice formed in MIS 24, perhaps due to seasonality effects originating in the Southern Hemisphere, before the renewed ice growth in MIS 22 yielded a very large ice sheet. We see no evidence of a pattern of cooling since 1500 ka, but near-freezing temperatures occur at every glacial maximum. The records over obliquity cycles before about 1 million years ago show a much weaker role for ice volume because of smaller ice sheets.

References and Notes

1. J. Chappell, N. J. Shackleton, *Nature* **324**, 137 (1986).
2. N. J. Shackleton, *Science* **289**, 1897 (2000).
3. N. J. Shackleton, *Nature* **215**, 15 (1967).
4. N. J. Shackleton, N. D. Opdyke, *Quat. Res.* **3**, 39 (1973).
5. P. U. Clark *et al*., *Quat. Sci. Rev.* **25**, 3150 (2006).
6. S. Sosdian, Y. Rosenthal, *Science* **325**, 306 (2009).
7. P. A. Martin *et al*., *Earth Planet. Sci. Lett.* **198**, 193 (2002).
8. H. Elderfield, J. Yu, P. Anand, T. Kiefer, B. Nyland, *Earth Planet. Sci. Lett.* **250**, 633 (2006).
9. J. Yu, W. S. Broecker, *Science* **328**, 1480 (2010).
10. S. Sosdian, Y. Rosenthal, *Science* **328**, 1480 (2010).
11. R. Bintanja, R. S. W. van de Wal, J. Oerlemans, *Nature* **437**, 125 (2005).
12. M. Siddall *et al*., *Quat. Sci. Rev.* **25**, 3185 (2006).
13. E. M. Gasson *et al*., *Rev. Geophys.* **50**, RG1005 (2012).
14. P. Kohler, H. Fischer, *Clim. Past* **2**, 57 (2006).
15. H. Elderfield *et al*., *Quat. Sci. Rev.* **29**, 160 (2010).
16. J. Jouzel *et al*., *Science* **317**, 793 (2007).
17. I. N. McCave, L. Carter, I. R. Hall, *Quat. Sci. Rev.* **27**, 1886 (2008).
18. T. Whitworth III *et al*., *Prog. Oceanogr.* **43**, 1 (1999).
19. L. E. Lisiecki, M. E. Raymo, *Paleoceanography* **20**, PA1003 (2005).
20. F. Parrenin *et al*., *Clim. Past* **3**, 485 (2007).
21. A. Martínez-Garcia *et al*., *Paleoceanography* **24**, PA1207 (2009).
22. D. A. Hodell, K. A. Venz, C. D. Charles, F. J. Sierro, in *Earth's Climate and Orbital Eccentricity: The Marine Isotope Stage 11 Question*, A. W. Droxler, R. Z. Poore, L. H. Burckle, Eds., *AGU Geophys Monogr.* **137**, 113–129 (2003).
23. V. Masson-Delmotte *et al*., *Quat. Sci. Rev.* **29**, 113 (2010).
24. W. G. Thompson, S. L. Goldstein, *Quat. Sci. Rev.* **25**, 3207 (2006).
25. A. L. Thomas *et al*., *Science* **324**, 1186 (2009).
26. J. F. Adkins, K. McIntyre, D. P. Schrag, *Science* **298**, 1769 (2002).
27. A. Sima, A. Paul, M. Schulz, J. Oerlemans, *Geophys. Res. Lett.* **33**, L15706 (2006).
28. M. Siddall *et al*., *Nature* **423**, 853 (2003).
29. D. Maraun, J. Kurths, M. Holschneider, *Phys. Rev. E Stat. Nonlin. Soft Matter Phys.* **75**, 016707 (2007).
30. D. Maraun, J. Kurths, *Nonlin. Processes Geophys.* **11**, 505 (2004).
31. D. Paillard, *Nature* **391**, 378 (1998).
32. P. D. Ditlevsen, *Paleoceanography* **24**, PA3204 (2009).
33. K. T. Lawrence, S. Sosdian, H. E. White, Y. Rosenthal, *Earth Planet. Sci. Lett.* **300**, 329 (2010).
34. M. E. Raymo, L. E. Lisiecki, K. H. Nisancioglu, *Science* **313**, 492 (2006).
35. T. Naish *et al*., *Nature* **458**, 322 (2009).
36. D. Pollard, R. M. DeConto, *Nature* **458**, 329 (2009).
37. R. McKay *et al*., *Quat. Sci. Rev.* **34**, 93 (2012).
38. M. E. Raymo, D. W. Oppo, W. Curry, *Paleoceanography* **12**, 546 (1997).
39. D. A. Hodell, K. A. Venz, C. D. Charles, U. S. Ninneman, *Geochem. Geophys. Geosyst.* **4**, 1004 (2003).
40. L. E. Lisiecki, *Geophys. Res. Lett.* **37**, L21708 (2010).
41. P. Wang, J. Tian, L. J. Lourens, *Earth Planet. Sci. Lett.* **290**, 319 (2010).
42. B. A. A. Hoogakker, E. J. Rohling, M. R. Palmer, T. Tyrrell, R. G. Rothwell, *Earth Planet. Sci. Lett.* **248**, 15 (2006).
43. K. A. Venz, D. A. Hodell, *Palaeogeogr. Palaeoclimatol. Palaeoecol.* **182**, 197 (2002).
44. N. J. Shackleton, In *Fate of Fossil Fuel CO_2 in the Oceans*, N. R. Anderson, A. Malahoff, Eds. (Plenum, New York, 1977) pp. 401-427.
45. I. R. Hall, I. N. McCave, N. J. Shackleton, G. P. Weedon, S. E. Harris, *Nature* **412**, 809 (2001).
46. A. M. Piotrowski, S. L. Goldstein, S. R. Hemming, R. G. Fairbanks, *Science* **307**, 1933 (2005).
47. B. Hönisch, N. G. Hemming, D. Archer, M. Siddall, J. F. McManus, *Science* **324**, 1551 (2009).

Acknowledgments: This work was funded in part by The Natural Environment Research Council (UK) and The European Research Council (ERC grant 2010-ADG-267931) and is a contribution to the European Project on Ocean Acidification (EPOCA), which received funding from the European Community's Seventh Framework Programme (FP7/2007-2013) under grant agreement no. 211384 and from the EPICA-MIS (Enhanced Palaeoreconstruction and Integrated Climate Analysis Through Marine and Ice Core Studies) program. Funding was also provided by a Royal Society Leverhulme Trust Senior Research Fellowship and a CORC-ARCHES (Consortium on the Ocean's Role in Climate/Abrupt climate Change Studies) Visiting Scientist post at Lamont Doherty Earth Observatory of Columbia University, for which H.E. is grateful to W. Broecker. We thank J. Firth and colleagues at the IODP core repository, College Station, for help in sampling ODP 1123. L. Booth and C. Daunt, and additionally J. Clegg, J. Day, M. Hall, J. Nicholson, N. Roberts, J. Rolfe, J. Smith, S. Smith, and S. Sounef-Ureta provided crucial laboratory support in Cambridge. We thank L. Booth and I. Weidle for their work on *Uvigerina* morphologies. G. Bayon, E. Ponzeve, and N. Freslon provided help during εNd analysis at IFREMER (Institut français de recherche pour l'exploitation de la mer) Brest, France. D. Maraun helped with use of Sowas software, and F. Joos, H. Pälike, R. Rickaby, T. Stocker, and G. Weedon helped with discussions. The reviews of the manuscript were very valuable, especially in encouraging us to focus on interpretation of the $\delta^{18}O_C$ record.

Supplementary Materials

www.sciencemag.org/cgi/content/full/337/6095/704/DC1
Materials and Methods
Supplementary Text
Figs. S1 to S15
Tables S1 to S3
References (*48–64*)

29 February 2012; accepted 25 June 2012
10.1126/science.1221294